EXHAUSTIVE GRAPH CUT-BASED VASCULATURE RECONSTRUCTION

Mathias Unberath[1,2]*, Stephan Achenbach*[3]*, Rebecca Fahrig*[4]*, Andreas Maier*[1,2]

[1]Pattern Recognition Lab, FAU Erlangen-Nürnberg, Germany
[2]Graduate School in Advanced Optical Technologies, Erlangen, Germany
[3]University Hospital, FAU Erlangen-Nürnberg, Germany
[4]Radiological Science Lab, Stanford University, Stanford, Germany

ABSTRACT

We propose an exhaustive extension to graph cut-based coronary artery reconstruction from multiple views of a rotational angiography sequence. The reconstruction is formulated as an energy minimization problem that is solved using the α-expansion algorithm. We enforce reprojection-based data consistency and completeness conditions on the reconstructed centerline. The proposed strategy omits the need for selection and manual refinement of a reference view.

A phantom study is used to assess the performance in 2D and 3D. The average reprojection error decreased from 1.32 ± 0.99 mm to 0.54 ± 0.02 mm. Moreover, an increase in Dice score from 0.50 ± 0.04 mm to 0.59 ± 0.00 mm was observed, indicating superior volumetric reconstruction quality. The results suggest that the proposed extension removes the susceptibility to reference frame selection and manual interaction, while increasing reconstruction quality.

***Index Terms*—** Graph Cut, Symmetrization, Cardiac Imaging, Epipolar Geometry, Cardiac Dynamics, C-arm CT

1. INTRODUCTION

To date, the diagnosis of cardiovascular disease relies on the analysis of X-ray coronary angiography [1]. To assess the complex structure of the coronary artery tree from 2D projection images, multiple frames have to be acquired from various viewing angles. Different magnifications, superimposition effects, and foreshortening complicate the assessment [2, 3]. Above-mentioned drawbacks can be overcome by 3D reconstruction of the coronary arteries from rotational angiography, improving assessment and guidance [4]. Due to the low temporal resolution of C-arm CT scanners straightforward reconstruction is unrewarding. Therefore, motion compensation strategies such as ECG-gating have to be incorporated into the reconstruction. However, ECG-gating yields sparse data leading to a strongly ill-posed reconstruction problem [5]. In backprojection-type reconstruction this issue is compensated for by use of a temporal window around the selected motion state [1]. While reducing undersampling artifacts this strategy introduces residual motion that corrupts image quality [1]. When using strict ECG-gating backprojection-type reconstruction becomes imperative as only few views remain. Blondel *et al.* proposed a method based on triangulation to reconstruct coronary artery centerlines from few projections [3]. They imposed a hard epipolar constraint to reduce the number of correspondence candidates and consequently computational complexity. Enforcing a hard epipolar constraint, however, is unfavorable for centerlines that are partially incomplete or coinciding with the epipolar line.

Liao *et al.* formulated coronary artery reconstruction as an energy minimization problem [6]. The energy function comprises a soft epipolar constraint and a 3D smoothness regularization, and can be efficiently optimized using the α-expansion algorithm based on graph cuts [6, 7]. However, this approach requires the selection and manual editing of a reference view that should exhibit minimal foreshortening and overlap, making the reconstruction susceptible to the choice of the reference frame. In order to overcome this limitation we propose an exhaustive extension to graph cut-based coronary artery reconstruction. We present quantitative results of a phantom study using Cavarev [8].

2. METHODS

2.1. Gating, 2D segmentation, and centerline extraction

In a typical rotational angiogram 133 frames covering $200°$ and the corresponding ECG-signal are acquired. ECG-gating for reference phase h_t relies on the cosine-based gating function $\lambda_a(h_t)$ defined as

$$\lambda_a(h_t) = \begin{cases} \cos^b\left(\frac{d(h_a,h_t)}{w}\pi\right) & \text{if } d\left(h_a, h_t\right) < \frac{w}{2} \\ 0 & \text{else,} \end{cases} \tag{1}$$

where h_a is the heart phase in the a^{th} projection image, $w \in [0, 1[$ controls the width and $b \geq 0$ controls the shape of the gating function [1]. We only retain frames with $\lambda_a(h_t) > 0.94$ yielding 5-8 frames depending on h_t, the scan duration, and the patient's heart rate.

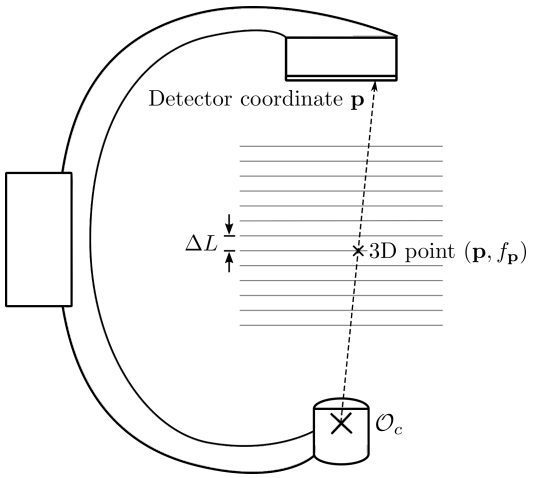

Fig. 1. Planes of equal depth are defined within the 3D field of view between the optical center $\mathcal{O}_c^{(r)}$ and the detector plane of the reference view I_r. A centerline point $\mathbf{p} \in Q_r$ can then be reconstructed if its depth label $f_\mathbf{p}$ is known.

The coronary arteries are segmented in the remaining projections I'_a, $a = 1, \ldots, A$. Contrasted vessels appear as small tubular structures with a larger scale background. Therefore, a morphological top-hat filter with a circular structuring element with radius R is used to remove all structures larger than the structuring element [1, 9]. We combine the top-hat filtered image $I_a^{\mathrm{TH}}(\mathbf{u})$ with the output $I_a^{\mathrm{V}}(\mathbf{u})$ of a multi-scale Hessian-based method to suppress responses from non-tubular structures [10]. The enhanced image is given as:

$$I_a(\mathbf{u}) = \begin{cases} I_a^{\mathrm{V}}(\mathbf{u}) & \text{if } I_a^{\mathrm{V}}(\mathbf{u}) > t_{\mathrm{V}} \wedge I_a^{\mathrm{TH}}(\mathbf{u}) > 0 \\ 0 & \text{else} \end{cases}, \quad (2)$$

where t_{V} is an empirically determined threshold. The image is then binarized by hysteresis thresholding.
The set of points Q_a defining the centerline in view a is obtained using morphological thinning followed by line segment pruning [11]. The strategy works well for the Cavarev data set. However, few line segments originating from non-vessel structures such as cortical rib bone persist in some views.

2.2. 3D centerline reconstruction

We assume that the projection matrices $\mathbf{P}_a \in \mathbb{R}^{3\times4}$ corresponding to the views I_a are known. Using the matrices $\mathbf{P}_a$ we can calculate the optical centers $\mathcal{O}_c^{(a)}$. A reference view I_r is selected and the field of view between the optical center $\mathcal{O}_c^{(r)}$ and the detector plane is divided into $l \in L$ planes of equal depth [6]. A schematic of the geometry is shown in Fig. 1. A 3D centerline point projected onto $\mathbf{p} \in Q_r$ must lie on the ray $\mathbf{r}_\mathbf{p} = \overline{\mathcal{O}_c^{(r)}\,\mathbf{p}^{3\mathrm{D}}}$ connecting the optical center and the 3D position of the centerline point $\mathbf{p} \in \mathbb{R}^2$. Therefore, if the depth label $f_\mathbf{p}$ of point $\mathbf{p}$ is known its 3D reconstruction $\mathbf{m}_\mathbf{p} \in \mathbb{R}^3$ is given by

$$\mathbf{m}_\mathbf{p} = (\mathbf{p}, f_\mathbf{p}) = \mathcal{O}_c + \frac{\mathbf{r}_\mathbf{p}}{\eta} \cdot \Delta L \cdot f_\mathbf{p}, \quad (3)$$

where $\eta = (\mathbf{r}_\mathbf{p}^\top \mathbf{r}_{\mathbf{p}_0})/(\mathbf{r}_{\mathbf{p}_0}^\top \mathbf{r}_{\mathbf{p}_0})$, $\mathbf{p}_0$ is the center pixel, and ΔL is the plane spacing.
We now want to find an optimal set of depth labels $\mathbf{f} \in \mathbb{R}^{|Q_r|}$ such that the reconstructed 3D points are in good agreement with the remaining views $I_{a\neq r}$ and piecewise continuous. The mapping $\mathbf{f}$ satisfying these requirements is obtained by minimization of an energy function:

$$E(\mathbf{f}) = \sum_{\mathbf{p}\in Q_r} D_\mathbf{p}(f_\mathbf{p}) + \beta \sum_{(\mathbf{p},\mathbf{q})\in\mathcal{N}} V_{\mathbf{p},\mathbf{q}}\left(f_\mathbf{p}, f_\mathbf{q}\right). \quad (4)$$

$D_\mathbf{p}$ encodes the soft epipolar constraint. To properly define projections we use underline notation to denote points expressed in homogeneous coordinates. Using $\underline{\mathbf{v}}_\mathbf{p}^{(a)} = \mathbf{P}_a\,\underline{\mathbf{m}}_\mathbf{p}$

$$D_\mathbf{p}(f_\mathbf{p}) = \frac{1}{A-1} \sum_{a\neq r} \min\left(\|\mathbf{v}_\mathbf{p}^{(a)} - c_a(\mathbf{m}_\mathbf{p})\|_2, k_1\right), \quad (5)$$

where $c_a(\mathbf{m}_\mathbf{p}) = \left\{\mathbf{q} \in Q_a \mid \min_\mathbf{q} \|\mathbf{v}_\mathbf{p}^{(a)}, Q_a\|_2\right\}$ is the centerline point $\mathbf{q} \in \mathbb{R}^2$ in view a closest to the projected point, and k_1 is a constant. The smoothness term $V_{\mathbf{p},\mathbf{q}}$ is defined over $\mathcal{N}$, the set of all 4-connected neighbors in Q_r:

$$V_{\mathbf{p},\mathbf{q}}\left(f_\mathbf{p}, f_\mathbf{q}\right) = \begin{cases} \min\left(\|f_\mathbf{p}, f_\mathbf{q}\|_2, k_2\right), & \text{if } \mathbf{p},\mathbf{q} \in B \\ \min\left(\|f_\mathbf{p}, f_\mathbf{q}\|_2, k_3\right), & \text{else} \end{cases}, \quad (6)$$

where B is the set of all branching points in Q_r, and $k_2 < k_3$ are constants. A smaller k_2 allows for discontinuities accounting for branching points that arise from projective simplifications. An efficient way of minimizing Eq. 4 is the α-expansion algorithm on graph cuts [6, 7]. A depth label mapping $\mathbf{f}$ lies within one α-expansion of $\mathbf{f}'$ if $f_\mathbf{p} = f'_\mathbf{p} \vee f_\mathbf{p} = \alpha \in L\ \forall \mathbf{p} \in Q_r$. Put concisely, for all labels $\alpha \in L$ we seek to find $\hat{\mathbf{f}} = \arg\min E(\mathbf{f}')$ within one α-expansion of the current mapping $\mathbf{f}$. As for particular points $\mathbf{p} \in Q_r$ the depth label $f_\mathbf{p}$ either changes to α or stays the same, each move is essentially a partitioning problem that can be efficiently solved using a graph cut [7]. A comprehensive description of the algorithm can be found in [6, 7].

2.3. Exhaustive extension and outlier removal

The method described above is robust against incomplete or inaccurate centerlines $Q_{a\neq r}$. Selection of the reference frame Q_r, however, drastically influences the reconstruction result. On the one hand only the centerline points present in Q_r can be reconstructed, suggesting best performance for views with minimal foreshortening and overlap. On the other hand all points in the reference view will be reconstructed favoring

views without redundant segmentations. Liao *et al.* addressed this issue by requiring manual selection and refinement of a reference frame. Instead, we propose an exhaustive extension to the reconstruction method that only marginally depends on the reference frame while being robust against incomplete or inaccurate centerlines in all views Q_a.

(i) Similarly to [3] we claim that correctly reconstructed points are in agreement with the majority of observations Q_a. This property is enforced by requiring $\mathrm{med}(\mathbf{m}_{\mathbf{p}_a}) \leq t_{2\mathrm{D}}$, where $t_{2\mathrm{D}}$ is a constant, $\mathbf{m}_{\mathbf{p}_a}$ is reconstructed from view a following the method described in Sec. 2.2, and

$$\mathrm{med}(\mathbf{m}_{\mathbf{p}_a}) = \mathrm{median}\left\{ \|\mathbf{v}_{\mathbf{p}_a}^{(j)} - c_j(\mathbf{m}_{\mathbf{p}_a})\|_2 \mid j \neq a \right\}.$$

Removing non-compliant points introduces robustness towards segmentation errors.

(ii) While the remaining points are in agreement with the majority of the views, the completeness of the reconstruction is not yet guaranteed. Therefore, we propose to incorporate all points $\mathcal{H}^{(a)} = \{(\mathbf{p}_a, f_{\mathbf{p}_a}) \,|\, \mathbf{p}_a \in Q_a \setminus \{c_a(\mathbf{m}), \mathbf{m} \in \mathcal{M}\}\}$ fulfilling (i) into the reconstruction. $\mathcal{M}$ denotes the current set of reconstructed centerline points.

In practice, an initial reconstruction is performed from an arbitrary centerline Q_{a_1} and all points with $\mathrm{med}(\mathbf{m}) > t_{2\mathrm{D}}$, $\mathbf{m} \in \mathcal{M}$ are removed. Then, either in a random or fixed order, the remaining centerlines $\mathcal{Q} = \{Q_a \,|a = 1, \ldots, A\} \setminus \{Q_{a_1}\}$ are used to complete the set of reconstructed points. In each step i, $\mathcal{H}^{(a_i)}$ is determined according to (ii) and added to the set of reconstructed points $\mathcal{M} = \mathcal{M} \dot{\cup} \mathcal{H}^{(a_i)}$, $\mathcal{Q} = \mathcal{Q} \setminus Q_{a_i}$. The procedure stops when $\mathcal{Q} = \emptyset$. Finally, points forming isolated point clusters of size n_c that lived through the refinement due to small reprojection errors are removed by requiring at least $\frac{n_c}{2}$ neighbors within a $\frac{n_c}{2}\Delta L$ neighborhood.

2.4. Symbolic reconstruction

The 3D centerline is reconstructed following Sec. 2.3 and a radius value is calculated automatically from the segmentations for each centerline point $r = \mathrm{median}\{r_a | a = 1, \ldots, A\}$, taking into account the magnification factor arising from the geometry. The symbolic representation is splatted into a volumetric grid to enable Dice score-based evaluation [8].

2.5. Experiments

The method introduced in Sec. 2.2 with and without its exhaustive extension were evaluated with respect to reconstruction accuracy, and overall quality, including completeness. Accuracy was assessed using the 2D reprojection error in a leave-one-out approach. The ground truth segmentation was obtained manually. Overall quality of the symbolic reconstruction was assessed using the Q3D measure based on the Dice coefficient [8], implicitly estimating the completeness of the reconstruction. The number of depth labels was chosen such that $\Delta L = 0.5\,\mathrm{mm}$. The constants were fixed to

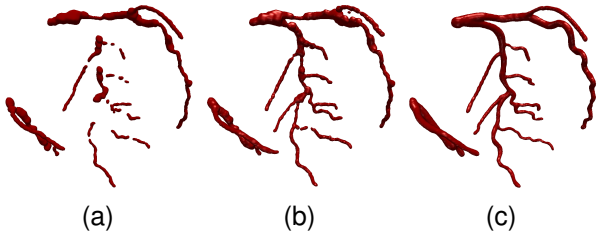

Fig. 2. Volume renderings of the symbolic reconstruction at $h_t = 0.9$ obtained using the original and the proposed method in Fig. 2a and 2b, respectively, and the ground truth Fig. 2c.

$k_1 = 20 \cdot \sigma = 6.2\,\mathrm{mm}$, $k_2 = 9.6\,\mathrm{mm}$, $k_3 = 32\,\mathrm{mm}$, $t_{2\mathrm{D}} = 2 \cdot \sigma = 0.62\,\mathrm{mm}$, and $n_c = 11$, where σ is the isotropic pixel spacing of the Cavarev data set. All reconstructions were performed at end diastole with $h_t = 0.9$.

3. RESULTS AND DISCUSSION

Results for the 2D reprojection error are shown in Table 1. Each column represents the error with respect to the projection excluded from the set used for the particular reconstruction. We stated the average reprojection errors, derived from the reconstruction of every remaining view as reference or initial frame. We found substantial reductions in both, the reprojection error and its standard deviation when applying the proposed extension. Low reprojection errors indicate proper reconstructions of the underlying 3D scenes. The discrepancy in the mean reprojection error between both methods likely arises from segmentation artifacts in the reference frame that propagated through the reconstruction. The method proposed here incorporates an outlier rejection step and a consistency condition $\mathrm{med}(\mathbf{m}) \leq t_{2\mathrm{D}}$ introduced in Sec. 2.3 that automatically mitigates such effects, while the original method required manual preprocessing [6]. Moreover, the standard deviation of the error for reconstructions from different views drastically decreased from 0.99 ± 0.61 mm to 0.02 ± 0.01 mm when using the proposed method. We believe that this result is more important, as it indicates that the reconstruction accuracy is independent from the reference frame. Nevertheless, some views contain more relevant information for the reconstruction than others. This property can be understood when comparing the reprojection errors stated in each column of Table 1, as they represent the results obtained by excluding distinct frames from the reconstruction.

The quality of the symbolic reconstruction was evaluated using Q3D, a two-sided measure assessing the spatial overlap of the volumetric reconstruction and the ground truth [8]. The proposed method resulted in an average Q3D of $0.59 \pm 0.00\,\mathrm{mm}$ being superior to the result obtained using the original method yielding $0.50 \pm 0.04\,\mathrm{mm}$. Points reconstructed with the original method $\mathcal{M}^{\mathrm{orig}}$ are included in

Omitted frame	0	1	2	3	4	5	6
Original method [mm]	0.84 $\pm$0.18	1.24 $\pm$0.63	1.25 $\pm$1.38	1.60 $\pm$1.75	1.82 $\pm$1.60	1.47 $\pm$0.97	0.99 $\pm$0.38
Exhaustive extension [mm]	0.62 $\pm$0.01	0.63 $\pm$0.02	0.53 $\pm$0.02	0.48 $\pm$0.02	0.46 $\pm$0.02	0.46 $\pm$0.00	0.60 $\pm$0.02

Table 1. Reprojection errors obtained using the leave-one-out scheme described in Sec. 2.5 for the original and exhaustive method. The error was averaged over the results of the reconstructions obtained from all possible reference frames.

the reconstruction result of the proposed extension, $\mathcal{M}^{\text{orig}} \subset \mathcal{M}^{\text{proposed}}$. Therefore, a higher Q3D value indicates a more complete reconstruction. Renderings of the symbolic volumetric reconstructions of both methods can be found in Fig. 2. The symbolic reconstruction obtained using the proposed method shown in Fig. 2b is in better agreement with the ground truth coronary artery tree shown in Fig. 2c. Liao *et al.* proposed the use of a minimum spanning tree in order to connect the 3D centerline points [6]. While a minimum spanning tree may be useful to compensate for small discontinuities of the vessels, applying the same strategy to fill large gaps in the reconstruction is objectionable as it enforces piecewise linear vessels. Although the proposed method results in a higher Q3D value it is evident from Fig. 2 that the volumetric representation requires improvement with respect to smoothness, continuity, and most importantly data fidelity in order to provide clinicians with images of diagnostic quality.

4. CONCLUSION

An exhaustive extension to graph cut-based coronary artery reconstruction from rotational angiography was introduced. In a phantom study, we found improved performance with respect to the reprojection error and a 3D Dice score-based metric. The reconstruction quality, consisting of accuracy and completeness, is largely independent from the choice of reference frame. Moreover, the proposed method is robust against statistically independent segmentation errors. The method does not require manual pre- or post-processing and can be applied in a fully automatic manner. Future work involves improvement of the volumetric reconstructions, and evaluation on clinical data sets. All algorithms are implemented in CONRAD, an open-source reconstruction framework [12].

Acknowledgment

The authors gratefully acknowledge funding of the Erlangen Graduate School in Advanced Optical Technologies (SAOT) in the framework of the German excellence initiative.

5. REFERENCES

[1] C Schwemmer, C Rohkohl, G Lauritsch, K Müller, and J Hornegger, "Residual motion compensation in ECG-gated interventional cardiac vasculature reconstruction.," *Physics in Medicine and Biology*, vol. 58, no. 11, pp. 3717–37, 2013.

[2] N E Green, S Y J Chen, A R Hansgen, J C Messenger, B M Groves, and J D Carroll, "Angiographic Views Used for Percutaneous Coronary Interventions: A Three-Dimensional Analysis of Physician-Determined vs. Computer-Generated Views," *Catheterization and Cardiovascular Interventions*, vol. 64, no. 4, pp. 451–459, 2005.

[3] C Blondel, G Malandain, R Vaillant, and N Ayache, "Reconstruction of Coronary Arteries from a Single rotational X-ray projection sequence.," *IEEE Transactions on Medical Imaging*, vol. 25, no. 5, pp. 653–63, 2006.

[4] J C Messenger, S Y J Chen, J D Carroll, J E B Burchenal, K Kioussopoulos, and B M Groves, "3D coronary reconstruction from routine single-plane coronary angiograms: Clinical validation and quantitative analysis of the right coronary artery in 100 patients," *The International Journal of Cardiac Imaging*, vol. 16, no. 6, pp. 413–427, 2000.

[5] B Desjardins and E A Kazerooni, "ECG-gated Cardiac CT," *American Journal of Roentgenology*, vol. 182, no. 4, pp. 993–1010, 2004.

[6] R Liao, D Luc, Y Sun, and K Kirchberg, "3-D reconstruction of the coronary artery tree from multiple views of a rotational X-ray angiography.," *The International Journal of Cardiovascular Imaging*, vol. 26, no. 7, pp. 733–49, 2010.

[7] Y Boykov, O Veksler, and R Zabih, "Fast approximate energy minimization via graph cuts," *IEEE Transactions on Pattern Analysis and Machine Intelligence*, vol. 23, no. 11, pp. 1222–1239, 2001.

[8] C Rohkohl, G Lauritsch, A Keil, and J Hornegger, "CAVAREV - An Open Platform for Evaluating 3D and 4D Cardiac Vasculature Reconstruction," *Physics in Medicine and Biology*, vol. 55, no. 10, pp. 2905–2915, 2010.

[9] E Hansis, D Schäfer, O Dössel, and M Grass, "Projection-based Motion Compensation for Gated Coronary Artery Reconstruction from Rotational X-ray Angiograms," *Physics in Medicine and Biology*, vol. 53, no. 14, pp. 3807, 2008.

[10] A F Frangi, W J Niessen, K L Vincken, and M A Viergever, "Multiscale vessel enhancement filtering," in *MICCAI 1998: 1st International Conference, Proceedings of the*. 1998, pp. 130—-137, Springer.

[11] T-C Lee, R L Kashyap, and C-N Chu, "Building skeleton models via 3-D medial surface axis thinning algorithms," *CVGIP: Graphical Models and Image Processing*, vol. 56, no. 6, pp. 462–478, 1994.

[12] A Maier, H G Hofmann, M Berger, P Fischer, C Schwemmer, H Wu, K Müller, J Hornegger, J-H Choi, C Riess, et al., "CONRAD – a software framework for cone-beam imaging in radiology," *Medical Physics*, vol. 40, no. 11, pp. 111914, 2013.